PIXE Analysis and Its Applications on Biological Materials

Stephen Mulware

Department of Mathematics and Science
United States Merchant Marine Academy
300 Steamboat Road, Kings Point, New York, 11024.

Disclaimer: The content of this work does not represent the views of the Department of Transportation, MARDA or the government of the United States.

Abstract:
Particle induced X-ray emission (PIXE) is a non-destructive ion beam analytical technique for elemental mapping and analysis using high energy ion beams as a probe and the characteristic X-rays of the sample elements as analytical signal. During PIXE heavy energy ions typically 1-4 MeV proton beams are used to induce element specific X-rays of the target sample of study. PIXE is surface sensitive due to the limited range of the impinging ions matter. With the advancement of microprobes with high focusing techniques, accelerated ion beams can be focused to 1μm level making PIXE one of the most effective analytical tools of detecting elements ranging from hydrogen to Uranium with up to ppm sensitivity, hence giving a clear picture of elemental distribution and composition of many samples including biological materials. In this paper, I will discuss the background process of PIXE analysis, sample preparation and report the results.

Keywords: Particle Induced X-ray Emission, inner shell ionization, trace elements and maps, microbeams.

1. INTRODUCTION:

PIXE is a non-destructive analytical technique that allows simultaneous multi-trace elemental analysis down to the ppm and even ppb sensitivity level. When high energy protons beam particles of the order of 1-4 MeV bombard target atoms, characteristic X-rays are emitted following the ejection of inner shell electrons and outer shell transitions. The energy of the emitted X-rays are the characteristics of the elements that make up the target and the intensities can be used to measure the abundance or concentration of a constituent element on the target. It is the most applied microanalysis techniques that have been used in many fields including chemistry, medicine, biology, agriculture, fisheries, industry, environmental studies of pollutants, mineral resources and archeological artifacts [1]. For a complete characterization of a multi-signal specimen, PIXE is often used in combination with methods such as Rutherford backscattering (RBS) and nuclear reaction analysis (NRA).

2. INNER SHELL IONIZATION OF TARGET ATOMS

When a typical MeV ion strikes a sample atom, the bombardment dislodges an inner shell electron creating a vacancy. MeV ions have high cross section for ejecting K, L, or M shell electrons because their velocities approach the inner shell electron velocities [2]. The unstable condition of the target atom cannot be maintained, and these vacancies are filled by outer-shell electrons. The outer shell electrons make a transition in energy by moving from a higher energy level to a lower energy level, and the difference in energy of the two levels can be released in the form of characteristic X-rays, whose energy identifies that atom. Therefore, the subsequent transition of an outer shell electron to fill up the created vacancy results in the emission of unique characteristic X-rays that identify the specific element of the target sample.

When an incident ion interacts with the target atom in a sample, it ejects an inner shell electron. In a competing process called Auger electron emission, this energy can also be transferred to another electron which is eventually ejected from the atom and can be detected by an electron detector. This observation implies that the step from ionization to X-ray production is not 100% efficient. This efficiency factor is known as the fluorescence yield and must be accounted for in analyzing the quantitative measurements of the elemental concentrations. The X-rays that are emitted from the sample are measured using an energy dispersive detector that has a typical energy resolution of ~2.5% (150 eV at 6 keV).

Conventionally, the transition filling vacancies in the innermost shell are called *K* X-rays, while those filling the second shell are *L* X-rays and those filling the third shell are M X-rays. The energies of the *L* X-rays are normally much lower than those of the *K* X-rays, and similarly *M* X-rays have much lower energies than the *L* X-rays. Due to the structure of the electron shells, there are naturally more possible transitions yielding *L* X-rays and even more possibilities of yielding *M* X-rays, and, therefore, it becomes more complex to measure the higher-order X-rays, and typically, the analytical method is limited to these three sets of X-rays from the elements. The limitation of detecting elements with Z<10 is due to the low energies of the soft X-rays from the light elements that are absorbed before reaching the detector. By placing a selection of filters in front of the detector, the high yield of low-energy X-rays that originate from the major elements of a sample can be filtered out. However, the technique does not provide depth distribution at which the emitted X-ray is produced since the X-ray energy measured does not give information of the depth even though the stopping of the bombarding ion is dependent on depth. The PIXE measurements are typically performed in the vacuum of a typical ion scattering chamber with ion currents in order nanoamperes. The low-beam current is meant to minimize beam damage of the samples, making PIXE a nondestructive analytical technique sensitive to trace-element concentration levels up to ppm or even ppb.

The binary collision between the incident ion projectiles and the target electrons will be considered first. The target electron mass will be expressed as m_e and that of the incident projectiles ions as m_p.The target electrons are bound in the sample atom with the energy given by $-U = \frac{1}{2}m_e v^2 - \frac{Ze^2}{r}$, (where U, r, v, Z and e are the binding energy, the distance from the nucleus, velocity of the electron at r, atomic number and elementary charge respectively). For a collision between an ion of velocity V and an electron, the transfer energy from the ion projectile to the electron is given by $2m_e V^2 + 2m_e vV$. The condition for ionization is given by $2m_e V^2 + 2m_e vV > U(: v > (U - 2m_e V^2)/(\,2m_e V)$. Only a low velocity projectile will cause ionization of electrons with large velocities. Thus, the inner shell ionization cross section drops with decreasing projectile energy $E(=\frac{1}{2}m_p V^2)$, which is approximately proportional to E^4. All electrons can be ionized under conditions of $2m_e V^2 > U: E > 4m_p U/m_e$. The ionization cross section is maximized at $E = 4m_p U/m_e$, and above this incident ion energy, the ionization cross section decreases as a function of $1/E$.

The inner shell ionization cross section σ^ican be estimated by binary encounter approximation based on Rutherford scattering between the electron and the incident ion projectile, and by using a classically calculated distribution considering that the inner shell electrons are bound by the Coulomb potential of the target atom as expressed in the equation below [3].

$$\frac{U^2\sigma^i(E,U)}{z^2} = f\left(\frac{m_e E}{m_p U}\right) \qquad (1)$$

Where z is the charge of the projectile. This is called the scaling law of the inner shell ionization cross section. Multiple inner shell ionization can occur in an ion-atom collision where an incident ion projectile simultaneously ionizes several inner shell electrons. For example, K-shell and L-shell multiple ionization is indicated by the satellite lines of K_α and K_β X-rays in the X-ray energy spectrum. The probability of multiple inner shell ionization as a function of impact parameter can be measured by perturbation theory based on semi classical approximation [4].

3. X-RAY PRODUCTION BY HEAVY CHARGED PARTICLE BOMBARDMENT

When inner shell ionization occurs due to heavy charged particle impacts (typically proton beams), the outer shell electrons transition to fill the vacancy producing a characteristic X-ray or Auger electron. The transition probabilities of the K_α X-rays, K_β X-rays and Auger electrons are denoted by Γ_α^X, Γ_β^X and Γ^A respectively. The emission ratio of X-ray ω is defined by the equation:

$$\omega = \frac{\Gamma_\alpha^X + \Gamma_\beta^X}{\Gamma_\alpha^X + \Gamma_\beta^X + \Gamma^A} \qquad (2)$$

where ω is called the fluorescence yield [5]. The value of ω is small in case of lighter elements.
The total production cross-section of K_α X-rays and K_β X-rays are thus expressed as:

$$\sigma K_\alpha^X = \frac{\Gamma_\alpha^X}{\Gamma_\alpha^X + \Gamma_\beta^X}\omega_K \sigma_K^i, \qquad \sigma K_\beta^X = \frac{\Gamma_\beta^X}{\Gamma_\alpha^X + \Gamma_\beta^X}\omega_K \sigma_K^i \qquad (3)$$

The total production cross section for L_α X-rays, L_β X-rays, and L_γ X-rays can be derived with a similar method. For ion beam energies less than 1MV, the differential production cross sections of L X-rays are slightly dependent on the emission angle in the direction in which the projectiles are incident, whereas those of the K X-rays are isotropic [6].

4. THE PRINCIPLE OF NUCLEAR MICROPROBE

The set-up of the nuclear microprobe used for PIXE begins at the ion source, which constitutes an important part of any Ion Beam Application (IBA) facility. The nuclear microprobe uses the interactions of an accelerated focused ion beam of MeV light ions with the target to determine local elemental concentrations. The major analytical techniques related to nuclear microprobe is usually based on the spectrometry of the X-rays and gamma-rays and the
scattered particles or those produced by nuclear reactions. Protons and helium particles
are the most frequently used particles for Rutherford Backscattering (RBS) and PIXE analysis. The other important components of a nuclear microprobe are the accelerator, the nuclear microprobe beamline, the focusing lens system, the sample chamber and detectors, the scanning system and the data acquisition and analysis system.

5. ACCELERATOR USED IN PIXE ANALYSIS

A small electrostatic accelerator or small cyclotron for accelerating proton beams to energies of a few MeV are typically suitable for PIXE analysis [1]. For the results discussed in this paper, the microprobe beamline at the NEC 9SDH tandem accelerator at the Ion Beam Modification and Analysis Laboratory (IBMAL) of the University of North Texas was used [7]. The tandem accelerator's analyzing magnet has a mass-energy-product of 500. Presently, there are four high-energy beam transport lines and one low-energy beam transport line taken from the ion source. One of the four high energy beamlines is the trace element accelerator mass spectrometer with a sensitivity in the order of parts per billion for many elements that was used for this research [8].

6. X-RAY DETECTOR FOR PIXE ANALYSIS

PIXE can be applied to trace element analysis due to the successful development of a high-resolution X-ray detector known as a HPGe – detector. A key factor in quantitative X-ray analysis using HPGe detector is the efficiency of the detector in use. This requires calculation or measurements of detection efficiency ε, as a function of X-ray energy. The absolute efficiency of a detector can generally be defined as the measure of how many pulses occur for a given number of X-rays striking its window. This efficiency is related to the specific source–detector geometry and the transmission and absorption properties of the detector [9]. It generally denotes the ratio of the number of counts produced by the detector to the total number of radiations emitted by the source. The intrinsic efficiency on the other hand is the ratio of the number of pulses produced by the detector to the actual number of X-rays striking the detector window. It considers the X-ray transmission through the beryllium entrance window of the cryostat a possible ice layer due to the cooling of crystal by liquid nitrogen and the absorption in the germanium active volume. For each experimental situation,

it is paramount to consider the solid angle of detection and any additional absorbing layers (75 µm polyethylene layer for our case) placed in front of the detector window.

7. APPLICATIONS OF PIXE IN ANALYZING BIOLOGICAL MATERIALS

The properties of many biological materials often depend on the spatial distribution and concentration of the trace elements present in a matrix. Various techniques including classical physical and chemical analyzing techniques each with relative level of accuracy have been used by many scientists before. However, with the development of spatially sensitive submicron beams, the nuclear microprobe techniques using focused proton beams for the elemental analysis of biological materials have yielded significant success. An analytical particle-induced X-ray emission (PIXE) procedure for mapping and multielement analysis of biological materials consists of several stages to yield reliable results. These include sample and specimen preparation, specimen bombardment, spectral data processing, quantification and correction for matrix effects [10]. Due to the spatial distribution of trace elements in many biological materials, critical aspects of the procedure must be considered, including contamination and/or losses during sample and specimen preparation and the danger of radiation or heat-induced losses during specimen bombardment.

8. TARGET SAMPLE PREPARATION FOR PIXE ANALYSIS

Two studies were conducted involving plants. The first study conducted was to investigate the effect of carbon nanotubes in iron uptake by plants. Quantitative analysis of iron uptake and distribution by corn roots germinated in different media some of which are laced with Fe (II) and Fe (III) of different concentrations, and carbon nanotubes (CNT) were done using µ-PIXE (particle induced X-ray emission spectrometry). The second study involved the investigation of the effect of using *arbuscular mycorrhizal fungi* in the roots of Mexican Marigold for phytoremediation to clean up Heavy Metal lead contaminated rhizosphere.

8.1 Corn Root Germination

Seeds of corn were germinated in vitro and in the dark in agarose gel medium. Besides the control group, there were also groups of seeds where the gel was spiked with solutions of Fe^{2+} and Fe^{3+} ions of different concentrations (1.0×10^{-3} Molar, and 3.0×10^{-4} Molar concentrations) with or without CNT. Fe (II) or Fe (III) was introduced as solutions of FeCl2 4H2O and FeCCl3-6H_2O respectively. Once the seeds germinated, they were fixed in paraformaldehyde solution.

8.2 Corn Root Preparation for Elemental Micro-Imaging

The root radical was excised about 5 mm long and inserted into a polyethylene tube of 5 mm diameter filled with tissue freezing medium, followed by immersion into liquid nitrogen cooled isopentane for rapid freezing. The frozen blocks with samples were then mounted on the sectioning dishes in a Leica cryostat CM 3050S. The temperature of the cryo-microtome head and the chamber were set at 25°C and 20°C, respectively. The samples were cryo-sectioned with thickness of 60 µm. The frozen sections were freeze-dried, mounted freestanding on aluminum frames for micro-PIXE analysis.

8.3 Mexican marigold phytoremediation with *arbuscular mycorrhizal fungi*

The *Tegetes erecta* (Mexican marigold) plants were grown symbiotically with or without *arbuscular mycorrhizal* fungus, *Glomus intraradices* in the presence or absence of Lead (Pb) at a level of 1000 mg per g dry substrate mass for a period of 9 weeks under the same conditions of temperature and humidity. Four categories of samples were prepared for analysis as follows:

(1) *Tegeres erecta* + *Mycorrhizal fungus* + lead [T + M + Pb]
(2) *Tegeres erecta* - *Mycorrhizal fungus* - lead [T - M - Pb]
(3) *Tegeres erecta* - *Mycorrhizal fungus* + lead [T - M + P]
(4) *Tegeres erecta* + *Mycorrhizal fungus* - lead [T + M - Pb]

Where (+) means presence of Mycorrhizal fungus or lead and (-) means absence of Mycorrhizal fungus or lead respectively. After nine weeks, the roots of the plants were excised about 5mm long, inserted in a tissue freezing medium inside a narrow plastic tube and quickly cryo-frozen in a container of isopentane (2-Methylbutane) cooled with liquid nitrogen. The samples were then frozen in a deep freezer at – 80°C for storage. The samples were removed, mounted on a mounting dish using a freezing medium and cryo-sectioned at a thickness of 60 µm. The sections were freeze-dried for about 2 hours, and then carefully mounted on aluminum sample holders ready for Particle Induce X-Ray Emission (PIXE).

9. ELEMENTAL MAPPING AND DISTRIBUTION OF THE CORN ROOTS FOR FE UPTAKE ANALYSIS

The PIXE elemental micro-imaging and analysis was done using a 2-MeV focused (5 µm spot size) proton beam. The average beam current of 50 pA was used to irradiate each sample with a scan area of 1 mm by 1 mm for 2 hours each. Simultaneous particle induced X-ray emission spectrometry (PIXE) and proton backscattering spectrometry (PBS) were performed using a Canberra GUL0110 HPGe X-ray detector with a resolution of 154 eV FWHM at 5.9 keV and a Canberra PIPS detector, respectively. The spectrometry system is calibrated for standard-free quantitative analysis [11]. From the PIXE data collected, quantitative elemental images mapping was done using GeoPIXE software package [12] that also provides the tools to extract elemental concentrations from regions of interest. Matrix correction is based on the information on the organic matric components extracted from PBS data using SIMNRA [13]. For each sample, several sections of the roots (n = 3 – 9) were analyzed and the concentrations averaged for the regions of interest which included the whole root, the epidermis, the cortex, the endodermis, and the vascular tissues. Figure 1 (a) and (b) below shows the PIXE spectrum, and the elemental maps of the corn root analyzed.

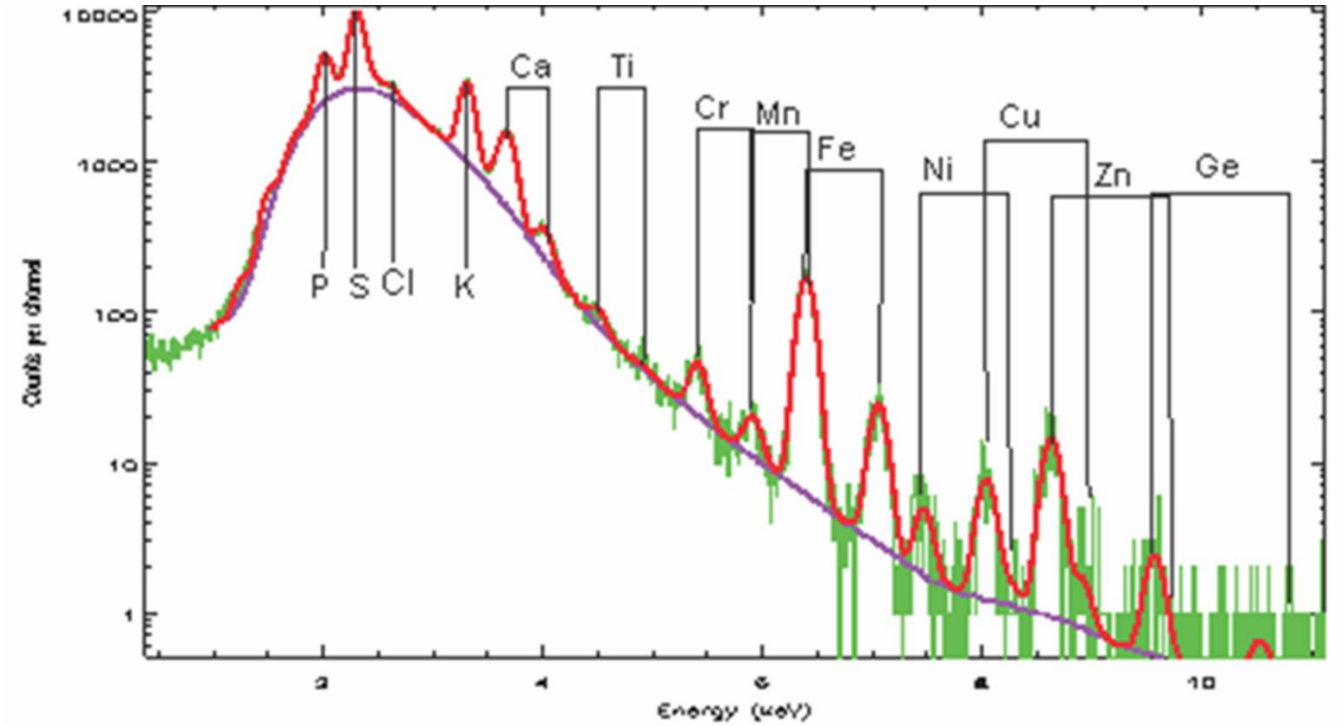

Figure 1(a) The PIXE spectrum for corn root

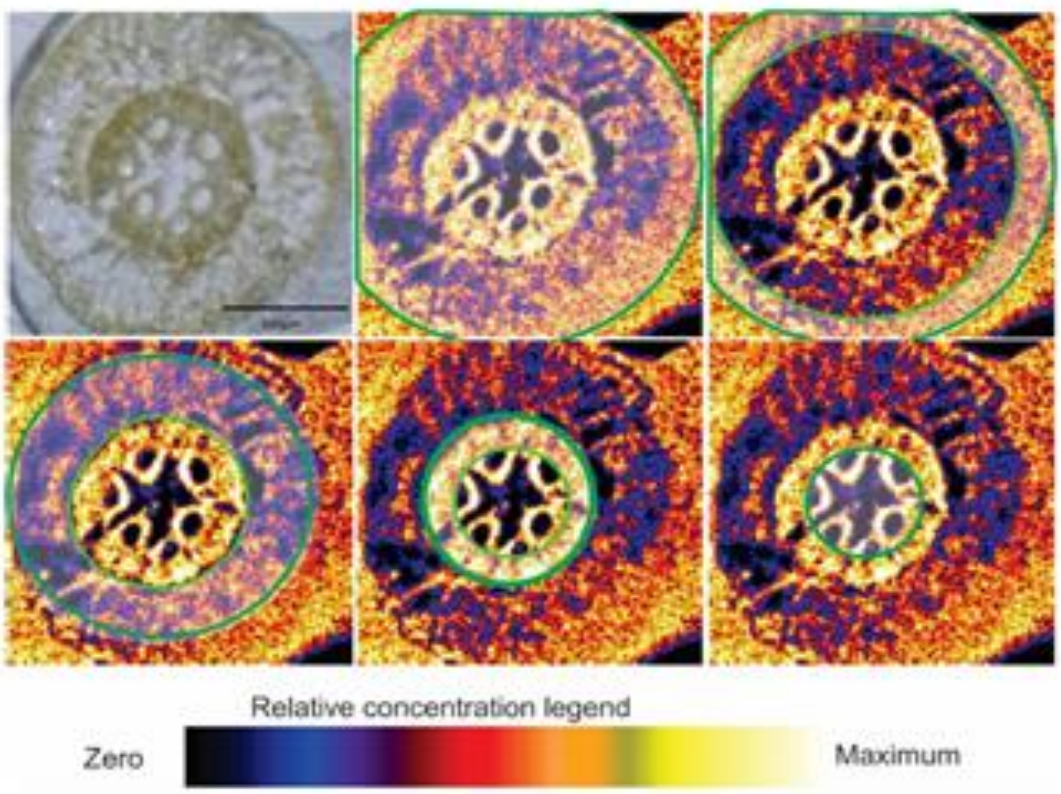

Figure 1(b) Elemental maps of the corn root sample showing the regions of interest. Top row: Optical image, whole root, epidermis. Second row: Cortex, endodermis, Vascular tissues. Scan size 250 × 250 Pixels; Scan width 1000 × 1000 µm.

10. ELEMENTAL MAPPING AND DISTRIBUTION OF THE CORN ROOTS FOR FE UPTAKE ANALYSIS

A 2.0 MeV proton beam from the Tandem accelerator was used for simultaneous PIXE and RBS measurements. The beam was focused to 5-µm diameter to strike a scan size of up to 1000 × 1000 μm^2 of the sample mounted on an aluminum holder. This beam spot was achieved with the object collimator set at 300 µm, and aperture collimator at 750 µm, and a beam current of 100 pA. The characteristic X-rays emitted from the target were measured by the HPGe-detector, which was mounted at 135^o with an effective solid angle of 203 msr. A 75 µm polyethylene filter was interposed in front of the detector to stop the back scattered protons. The cumulative charge from the analysis of the RBS data was used to analyze the PIXE spectra for elemental distribution on the samples irradiated.

For the elemental maps and concentration analysis, a dynamic analysis (DA) matrix of the fitted PIXE spectrum was generated and used to generate the elemental maps and concentrations using Geo-PIXE software. Figure 2(a) shows a typical PIXE spectrum of the Mexican marigold root obtained and the associated elemental maps. The PIXE data was analyzed to determine the elemental concentrations in the whole root section irradiated. Figure 2(b) shows the elemental distribution maps of an irradiated root sample.

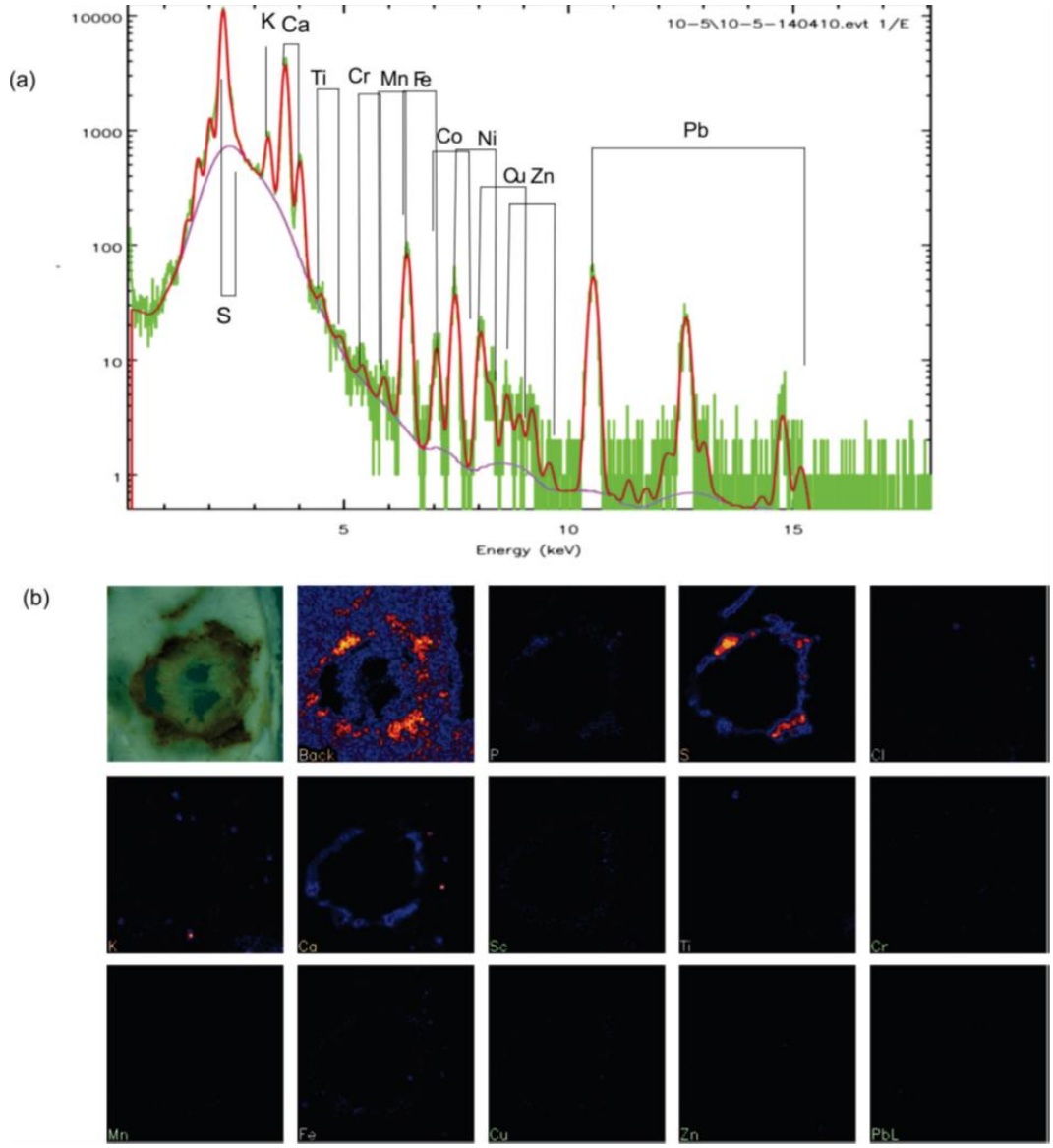

Figure 2 (a) Fitted micro-PIXE spectrum of the whole Tegetes erecta root, (b) Elemental maps of the Tegetes erecta root sample. Scan 250×50 pixel; Scan width 1000 ×1000 µm. The first image is the optical image.

11. RESULTS AND DISCUSSION

(a) Effect of Carbon nanotube in Iron Uptake by Corn Roots

Elemental concentrations were extracted from the images in five different regions of interest: the whole root, the epidermis, the cortex, the endodermis and the vascular tissues. The determination of elemental concentrations in different regions of the root tissue enables the comparison of the elemental concentrations and distribution in roots germinated in different media, and/or to assess the shifts in elemental depositions caused by the presence or absence of Fe (II), Fe (III), and CNT in the germinating media of each sample as described by Scheloske *et al.* [14]. µ-PIXE analysis revealed the presence of P, S, Cl, K, Ca, Ti, Cr, Fe, Cu, Zn, and As. In addition to the element of interest Fe, the concentrations of P and S recorded were the highest for each root across the samples tested. Figure 3(a) summarizes the results of the average P, S and Fe concentrations in ppm, measured by the µ-PIXE in the Epidermis and the endodermis of various root samples. Fe (II) enrichment of a medium helps to increase iron uptake by corn roots. In the presence of CNT, the uptake is more efficient as was found in this study. A higher Fe (II) concentration in the medium does not necessarily mean a higher uptake since Fe-deficiency stress mechanisms may compensate for lower Fe availability and achieve similar Fe uptake comparatively as with higher Fe concentration in the soil. Since Fe-uptake is highly regulated by plants, the results of this study can act as a model for building up a strategy to mitigate Fe-deficiency in cornfields.

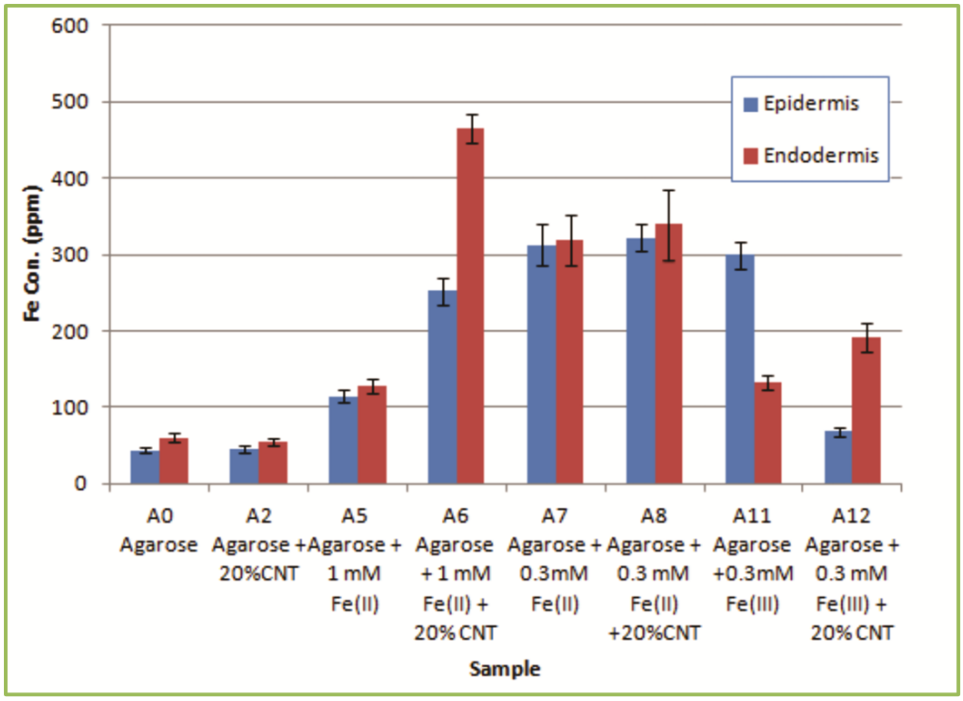

Figure 3(a) Results of role of CNT on Iron uptake by corn roots

(b) Effects of *arbuscular mycorrhizal fungus* on Lead phytoremediation

The *Tegetes erecta* plant that was grown symbiotically with *arbuscular mycorrhizal fungi* in a soil contaminated with lead extracted large amounts of Pb from their rhizosphere. Heavy metals (HM) are taken up by the plants through specific uptake systems but when present in high concentrations, they can enter the plant root system by non-specific transporters. Heavy metals can enter the root system through passive diffusion as well as though low-affinity metal transporter with broad specificity [15]. To maintain ion homeostasis's while growing in high HM concentration environment, plants rely on circumventing the generation of physiologically intolerable concentrations of these metals within the cells by regulating acquisition, enrichment, transportation and detoxification of the same [16,17]. Through extra-cellular HM-chelation mechanism by the root exudates as well as binding of HM to the rhizodermal cell walls, plants carry out the detoxification process. The chelating agents such as phytochelatins and metallothionein having high affinity of HM binding properties are extra-cellular generated by the plants cells to chelate the HM and export them from the cytoplasm across the tonoplast to be excreted inside the vacuole and other storage organelles [17]. Thus, by forming a network that acts as extension of the root system, the arbuscular mycorrhizal fungus enhanced the uptake of the Pb by the root as seen in our results. This effect is contrasted by a lower Pb concentration observed in the roots of the plants grown in Pb contaminated rhizosphere without the mycorrhizal fungus. Figure 3(b) shows the results of the analysis.

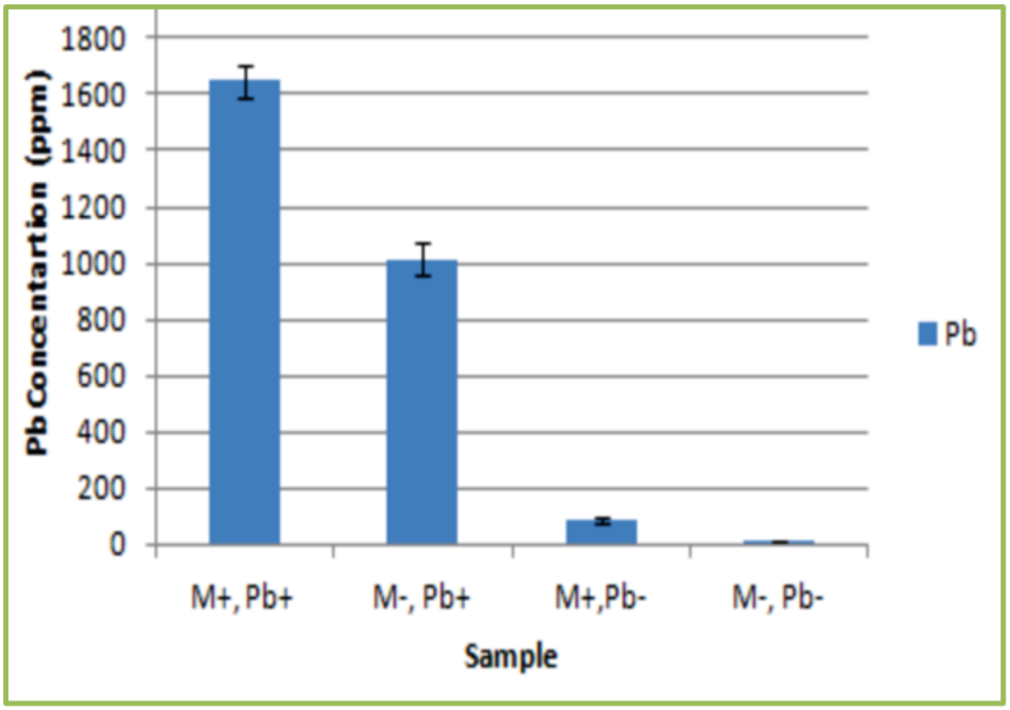

Figure 3(b) Results of the Lead Phytoremediation effects of arbuscular mycorrhizal fungi in the roots of Mexican Marigold.

CONCLUSION

The results presented here show that the PIXE analysis is now sufficiently sophisticated technology and is highly suitable for the analysis of biological samples. The results show that with careful sample preparation and correct ion beam application, PIXE analysis can accurately give a correct elemental mapping and concentration analysis of biological materials to give a more comprehensive understanding of elemental composition of the samples hence suitable for various biological studies.

REFERENCES:

1. Keizo Ishii, PIXE and its applications to elemental analysis, Quantum beam science, 2019.
2. Stephen Mulware, Review of Nuclear microscopy techniques: An approach for non-destructive Trace elemental analysis and mapping of biological materials. Journal of Biophysics, 2015.
3. Garcia, J. D. Inner shell ionizations by proton impact. *Phys. Rev. A* 1970, 1, 280-285.
4. Hansteen J. M., Mosebekk O. P. Atomic Coulomb excitation by heavy charged particles. *Nucl. Phys. A* 1973, 201, 541-560.
5. Kamiya, M.; Kinefuchi, Y.; Kuwako, A.; Ishii, K.; Morota, S. Projectile energy dependence of L_α to L_γ X-rays produced by proton and ^{3}He impacts on Ho and Sm. Phys. Rev. A 1979, 20 1820.
6. David N. Jamieson, Mark B. H. Breese, and Philip J. C. King, Materials Analysis Using a Nuclear Microprobe, John Wiley and Sons Ltd.
7. F. D McDaniel, J. L Duggan, C. Yang, B. N Guo, M. El Bouanani, and M. Nigam, "The high-energy heavy ion nuclear microprobe at the University of North Texas", Nuclear Instruments and Methods in Physics Research Section B: Beam Interactions with Materials and Atoms 181 (2001), no. 14, 99-103.
8. Bibhudutta Rout, Mangal S. Dhoubhadel, Prakash R. Poudel, Venkata C. Kummari, Bimal Pandey, Naresh T. Deoli, Wickramaarachchige J. Lakshantha, Stephen J. Mulware, Jacob Baxley, Jack E. Manuel, Jose L. Pacheco, Szabolcs Szilasi, Duncan L. Weathers, Tilo Reinert, Gary A. Glass, Jerry L. Duggan, Floyd D. McDaniel; An overview of the facilities, activities, and developments at the University of North Texas Ion Beam Modification and Analysis Laboratory (IBMAL). *AIP Conf. Proc.* 3 July 2013; 1544 (1): 11–18. https://doi.org/10.1063/1.4813454
9. Stephen J. Mulware, Jacob D. Baxley, Bibhudutta Rout, Tilo Reinert, Efficiency calibration of an HPGe X-ray detector for quantitative PIXE analysis, Nuclear Instruments and Methods in Physics

Research Section B: Beam Interactions with Materials and Atoms, Volume 332,2014, Pages 95-98, ISSN 0168-583X, https://doi.org/10.1016/j.nimb.2014.02.037.

10. Maenhaut W. Multielement analysis of biological materials by particle-induced X-ray emission (PIXE). Scanning Microsc. 1990 Mar;4(1):43-59; discussion 59-62. PMID: 2195651.
11. S. J. Mulware, J. D. Baxley, B. Rout, and T. Reinert, "Efficiency calibration of an HPGe X-ray detector for quantitative PIXE analysis", Nuclear Instruments and Methods in Physics Research Section B: 322 (2014), 95-98.
12. C. G. Ryan, "Quantitative trace element imaging using PIXE and the nuclear microprobe". Int. J. Imaging Syst. Technol., 11: (2000), 219–230.
13. M. Mayer, SIMNRA, a simulation program for the analysis of NRA, RBS and ERDA, AIP Conference Proceedings 475 (1999), no. 1.
14. S. Scheloske, M. Maetz, T. Schneider, U. Hilderbrandt, H. Bothe and B. Povh, "Element distribution in mycorrhizal and non-mycorrhizal roots of the halophyte Aster tripolium determined by proton induced X-ray emission," Protoplasm, vol. 223, pp. 183-189, 2004.
15. J. L. Hall and Lorraine E. Williams, Transition metal transporters in plants, Journal of Experimental Botany 54 (2003), no. 393, 2601-2613.
16. Elizabeth P. Colangelo and Mary Lou Guerinot, "The Essential Basic Helix-Loop-Helix Protein FIT1 Is Required for the Iron Deficiency Response", the Plant Cell Online 16 (2004), no. 12, 3400-3412.
17. Barry Halliwell and John M.C. Gutteridge, "Biologically relevant metal ion-dependent hydroxyl radical generation an update", {FEBS} Letters 307 (1992), no. 1, 108-112.